

Linear friction welding of dissimilar AA6082 and AA2011 aluminum alloys: microstructural characterization and design guidelines

Gianluca Buffa¹ · Marco Cammalleri¹ · Davide Campanella¹ · Umberto La Commare¹ · Livan Fratini¹

Received: 1 September 2015 / Accepted: 16 December 2015
© Springer-Verlag France 2015

Abstract This paper presents the results of an experimental and numerical campaign on Linear Friction Welding of dissimilar AA2011-T8 and AA6082-T6 aluminum alloys. Experimental tests were carried out with constant oscillation amplitude and process time. Varying oscillation frequency, interface pressure, specimen geometry and mutual position were used. Grain size measurements, HV tests and EDX analysis were considered to characterize the microstructure of the joints as a function of the input process parameters. A thermal numerical model was utilized to predict the temperature profiles in the joints during the process. The obtained results allowed the identification of four weld categories: sound joints, “bonding limit” condition and two different unwelded joints. The investigation of the causes of the different joint behavior permitted to obtain a few design guidelines on the LFW of dissimilar alloys with different geometry.

Keywords Linear Friction Welding · Dissimilar welds · Aluminum alloys · Grain size

Introduction

Linear Friction Welding (LFW) is a solid state welding process developed to join bulk parts. Similarly to the other friction based solid state welding processes, namely Rotary Friction Welding (RFW) and Friction Stir Welding (FSW), the material to be welded is softened by the friction forces

work decaying into heat. In particular, RFW is used to join axisymmetric parts [1] while FSW is used to join sheets metal in different configurations, i.e. butt, lap, T, spot, by a non consumable tool [2].

The LFW mechanics can be described by dividing the process into four steps [3]. In the first step, a reciprocating motion is activated and a compression force is given to the specimens, perpendicularly to the motion direction, in order to generate contact between the parts. During this step, the asperities on the contact surfaces are eliminated and the actual contact surface becomes equal to 100 % of the theoretical one. During the second step, temperature increases due to the friction forces work decaying into heat and material softening begins. During the third stage, the material is no longer able to bear the pressure applied and axial shortening is observed together with flash formation along the sides of the contact surfaces. During this stage the two specimens behave as a unique part and the material flows under the shear stress applied as demonstrated by Turner et al. [4]. Finally, during the last step, the reciprocating motion is quit and an additional forging pressure is applied to consolidate the weld.

LFW was patented in 1929 by Walther Richter (Germany) [5]. However, the process was considered by industry and academia as “very doubtful” due to the unclear description of the parts motion and the difficulties in building proper machines. The process potential was reconsidered during the 90s thanks to the development of the first dedicated machines at reasonable costs. In this way, LFW can be considered a relatively new process. As a solid state process, LFW is characterized by a number of advantages with respect to traditional welding processes [3]. In the LFWed joints, no porosities, inclusions, and weld contamination are observed. Oxides at the contact interface before the process are expelled as flash leaving the bonding area free of any inclusion. Additionally, the microstructure of the welded zone is characterized by fine

✉ Gianluca Buffa
gianluca.buffa@unipa.it

¹ Department of Chemical, Management, Computer Science, Mechanical Engineering, University of Palermo, Palermo, Italy

and equiaxed grain due to the recrystallization phenomena taking place during the process. Finally, as a consequence of the reduced heat input with respect to traditional fusion welding techniques, residual stresses and distortions are minimized [6]. A few process parameters influence the soundness of the produced joints by determining the heat input to the weld, namely oscillation frequency and amplitude, forging pressure and process time.

Research and industrial applications of LFW initially focused on titanium alloys and nickel based superalloys. In particular, Vairis and Frost studied the effect of the process parameters on the mechanical properties of Ti6Al4V joints and highlighted the features needed by the machine in order to produce sound joints [7, 8]. In their review paper, Chamanfar et al. highlighted the microstructural features, texture development, residual stresses, and mechanical properties of similar and dissimilar polycrystalline and single crystal Ni-based superalloy [9]. Main application for these materials is the so-called “blisks” of gas turbines in the aerospace and power generation fields. However, LFW can be successfully applied also to other materials as steels, magnesium alloys, copper and aluminum alloys. Fratini et al. studied the LFW of ASTM A285 steel using both experiments and a dedicated numerical model, finding proper combinations of process parameters in order to produce sound joints [10]. As far as aluminum alloys are regarded, only few papers have been published in the last few years. Song et al. studied from a numerical and experimental point of view the distribution of the residual stresses in similar AA2024 joints through synchrotron X-ray diffraction [11]. Jun et al. measured the residual strains in both similar AA2024 and dissimilar AA2024/AMC225xe joints by experimental diffraction measurements and eigenstrain reconstruction analysis [12]. Fratini et al. studied the bonding conditions, as a function of the process input parameters, occurring in LFW of similar AA6082 joints [13].

In the most recent years, research activity on LFW is focusing on the investigation of the possibility to produce dissimilar joints, thus fully exploiting the potential of the process. Different alloys can be considered for these applications. In particular, Ma et al. produced LFW joints out of dissimilar Ti6Al4V and Ti6.5Al3.5Mo1.5Zr0.3Si alpha + beta titanium alloys. The microstructure and the mechanical properties of the sound welds were examined and tensile strength comparable to the one of the parent Ti6Al4V was obtained [14]. Guo et al. studied a different couple of alpha + beta titanium alloys, namely Ti6Al4V and Ti6Al2Sn4Zr6Mo. An increase of the hardness with respect to the parent material was obtained in the Ti6Al4V side while a decrease was measured in the Ti6Al2Sn4Zr6Mo side. After post welding treatment, similar hardness values were reached [15]. Li et al. carried out an experimental campaign on LFW and Inertia Friction Welding on dissimilar nickel based superalloys. The fatigue resistance of the obtained joints was comparable to the one

of the weaker alloy [16]. As far as aluminum alloys are regarded, Wanjara et al. focused their research on the LFW of dissimilar AA6063 aluminum alloy and copper. Both process feasibility and the interface properties were investigated. A quite large process window was identified indicating that LFW can be considered as an effective alternative to Explosive Welding (EW) to join these metals, provided that sufficiently thick parts are considered. As a matter of fact, LFW cannot be used to join this sheets because of difficulties in the parts clamping. Although smaller intermetallic layer was found in the LFWed joints with respect to the EWed ones, the intermetallic layer grew after heat treatment and industrial service [17, 18]. Bhamji et al. carried out an experimental campaign on dissimilar LFW of pure copper and aluminum finding very good electrical and mechanical properties of the joints [19]. Some of the authors of the previous paper also studied the feasibility of the LFW process applied to aluminum and magnesium alloys. In particular, a dissimilar joint was produced out of AA6082 and AZ31 specimens. Satisfactory results were obtained in terms of yield strength of the joints with respect to the parent materials in the “O” state. Additionally, the presence of intermetallics and their detrimental effects on the joints mechanical properties were highlighted [20]. Finally, dissimilar aluminum to aluminum joints were studied by Rotundo et al. [21]. In their paper, the authors showed the feasibility of LFW between AA2024 and a 2124/25 vol% SiCp composite. High joint efficiency was reached, with UTS and YS equal to the 90 % of the base material. Additionally, uniform particle distribution was found in the 2124/25 vol% SiCp composite side. The lack of specific know-how represents one of the main causes of the scarce use of LFWed aluminum parts in industrial fields as aeronautics and ground transportation. In these sectors, in order to optimize mechanical strength and weight, a large use of light structures made of dissimilar alloys is needed to minimize fuel costs and meet the increasingly demanding environmental regulations on emissions. In particular, aluminum alloys as 2XXX, 6XXX and 7XXX series are considered in the above areas because of their good mechanical properties and corrosion resistance [22, 23].

In this paper, the results on a combined experimental and numerical study on LFW of dissimilar AA2011 and AA6082 aluminum alloys joints are presented. A dedicated in house built prototypal machine was used for the experiments. The process feasibility was investigated and a process window was obtained with varying oscillation frequency, forging pressure and mutual position of the specimens. The last variable was introduced to take into account the different geometry of the parts to be welded. The microstructure of the obtained joints was characterized by optical observation and EDX analyses. Microhardness was measured in a transverse section of the joints to highlight the modifications induced by the process. Finally, a thermal numerical model was set up and utilized to

Table 1 Composition of the used alloys (wt%).

Alloy	Si	Fe	Cu	Mn	Mg	Cr	Zn	Ti	Al
2011	0.5–1.2	0.7	5.0	0.4–1.2	0.2–0.8	0.1	0.25	0.15	remainder
6082	0.7–1.3	0.5	0.1	0.4–1	0.6–1.2	0.25	0.2	0.1	remainder

explain the different behavior of the joints with varying specimens geometry and mutual position. The aim of the present paper is to reduce the lack of knowledge regarding the influence of specimen geometry in a LFW process of different aluminum alloys.

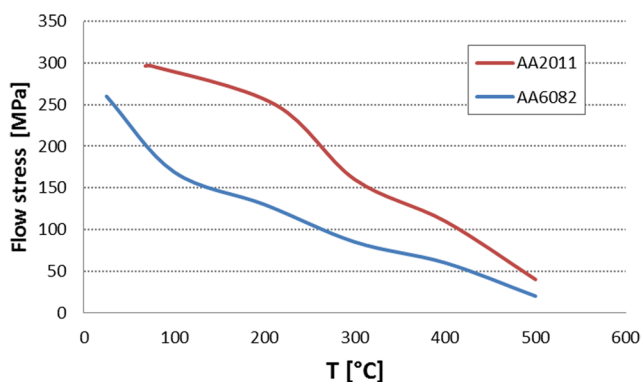
Materials and methods

Experimental set up

As specified in the introduction, the two aluminum alloys taken into account were AA2011-T8 and AA6082-T6. The composition of the two utilized alloys is reported in Table 1.

During the process, temperature increases significantly due to the friction forces and deformation work decaying into heat. Maximum temperature at the interface can reach 80–90 % of the melting temperature of the processed material. For this reason, especially when two different alloys are welded together, it is important to know the influence of temperature on the material flow stress. From Fig. 1 it is seen that AA2011 has a larger flow stress both at room temperature and, at a greater extent, at the typical process temperature, i.e. in the range of 200–450 °C [24].

The used specimens were CNC machined from bars having cross section 20 mm × 20 mm. The specimen geometry can be divided into two parts: a base, intended to be fixed by screws to the machine supports and the actual element to be welded, whose dimensions are different between the bottom and top specimen (Fig. 2). In particular, the bottom specimen has height 10 mm, length 10 mm and width 10 mm, while the top specimen has height 10 mm, length 10 mm and width 7 mm. This choice was made to highlight the effect of

**Fig. 1** Flow stress vs. temperature for the used aluminum alloys

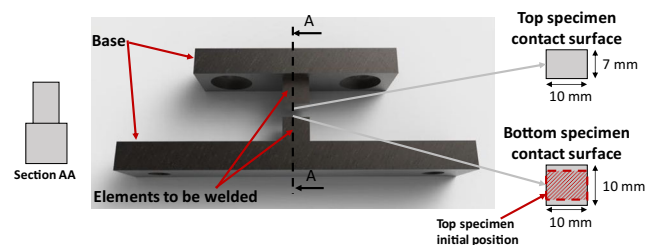
different geometries on the effectiveness of the obtained welds. It is worth noticing that for a number of industrial applications it is not possible to weld two parts with the same geometry and in particular with the same contact surface. On the other hand, the different heat capacity of the parts can affect the integrity of the produced weld. Figure 2 shows a sketch of the top and bottom specimen geometries.

The LFW experiments were carried out on a dedicated prototypal machine designed, built and developed by some of the authors during the last few years [10]. Figure 3 shows a sketch of the utilized machine.

The reciprocating motion of the bottom specimen is created using a desmodromic kinematic: two three-lobe cams are in contact with the plates from the two sides of the machine. It is worth pointing out that the high thermal conductivity of aluminum alloys requires large oscillation frequency values. In this way, three-lobe cams are needed in order to increase the range of frequencies available. Proper pressure was applied on the top specimen via a double-acting hydraulic actuator, fixed on a steel rack and controlled by an electro-valve, allowing loads up to 15,000 KN. A pneumatic clutch was positioned on a secondary shaft and connected to the main cam shaft in order to stop the oscillation when the assigned process time was reached. Further details on the machine can be found in [13].

During the experimental campaign, process time (t) and oscillation amplitude (A) were kept constant to 2.25 s and 3 mm, respectively. Oscillation frequency (f) and pressure at the interface (p) were varied according to Table 2, which summarizes the considered process parameters.

Each test was repeated three times. In order to analyze the integrity, the mechanical properties and the microstructure of the produced joints, cross sections were cut from each weld. The obtained specimens were hot mounted, polished and finally etched with Keller reagent for 15 s. Microhardness was measured and an optical microscope was used to highlight the grain dimensions in the different joint zones. Finally, EDX (Energy-dispersive X-ray spectroscopy) analyses were carried

**Fig. 2** Top and bottom specimen geometry

out using a scanning electron microscope in order to highlight the chemical composition along the cross section of the joints.

Numerical thermal model

A numerical model was used to calculate the temperature at the contact interface starting from an assigned heat flux conferred to the contact interface of the specimen. The commercial FEA software DEFORM-3D™, Lagrangian implicit code designed for metal forming processes, was used to model the thermal problem. Mechanical deformation was not taken into account in this model. As far as the thermal problem is regarded, the heat generation and transfer is expressed in the form of energy balance as follows,

$$K_1 T_{,ii} + \dot{r} - \rho c \dot{T} = 0 \quad (1)$$

where $k_1 T_{,ii}$ represents the heat transfer rate, r the heat generation rate and $\rho c \dot{T}$ the internal energy-rate.

The energy balance is written in the variation form

$$\int_V K_1 T_{,i} \delta T dV + \int_V \rho c \dot{T} \delta T dV - \int_V \alpha \sigma_{ij} \varepsilon_{ij} \delta T dV - \int_S q_n \delta T dS = 0 \quad (2)$$

where α is the fraction of mechanical work decaying into heat. This is not considered in this model as the energy input in the material, obtained from experimental measurements according to the procedure explained in [25], contains already the deformation energy fraction. In particular, the instantaneous inlet power was obtained starting from acceleration, torque and velocity measurements. The two components of the inlet power were then identified, namely the welding power (the power needed to apply the shear force at the interface between the specimens) and the lost friction power. The heat input to the thermal model was equal to the welding power. In this way, it was assumed that both the friction forces work and the entire deformation work decay into heat. This assumption can be considered reasonable for most metals, for which the energy lost for microstructural change is negligible with respect to the two above cited energies. As a consequence, no deformation is considered in the thermal model as the heat coming from the deformation during the process was already been

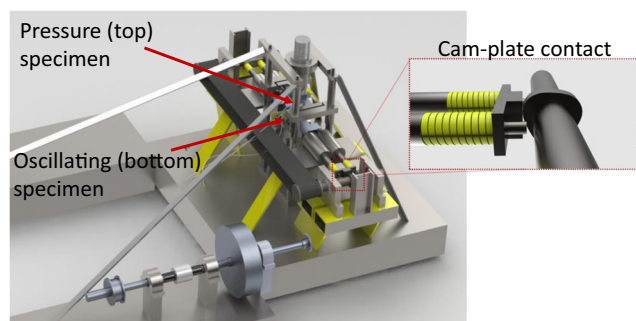


Fig. 3 Sketch of the utilized LFW machine

Table 2 Process parameters values.

f [Hz]	45, 60, 72
p [MPa]	20, 30, 40, 50, 60
t [s]	2.25
A [mm]	3

accounted for through the calculation of the welding power. q_n is the heat flux across the boundary surface S ,

$$q_n = k_q T_{,n} \quad (3)$$

Where k_q is conductivity of the q element and $T_{,n}$ is the temperature of the n node. To solve problems of this nature, it is required that the temperature field satisfies the prescribed boundary conditions and Eq. (3) for arbitrary perturbation δT . The finite element formulation for temperature analysis can be expressed as

$$[C]\{\dot{T}\} + [K_c]\{T\} = \{Q\} \quad (4)$$

being $[C]$ and $[K_c]$ the matrixes representing the thermal capacity and conductivity of the body, respectively. Temperature is often found by the finite difference approximation

$$T_{t+\Delta t} = T_t + \Delta t[(1-\beta)\dot{T}_t + \beta\dot{T}_{t+\Delta t}] \quad (5)$$

The convergence of Eq.(5) depends on the choice of the parameter β . It is usually considered that β should be larger than 0.5 to ensure an unconditional stability and a value of 0.75 is commonly selected [26].

The experimental specimen was meshed, for thermal analysis only, with about 15,000 tetrahedral elements. An external heat flow was assigned as boundary condition to the fraction of the surface in contact with the top specimen (red area in Fig. 4). The methodology used to calculate the heat flux is fully described in paper [25]. Thermal exchange with environment boundary condition was assigned to all the other surfaces of the specimen. Figure 4 shows the bottom specimen mesh used for the thermal model.

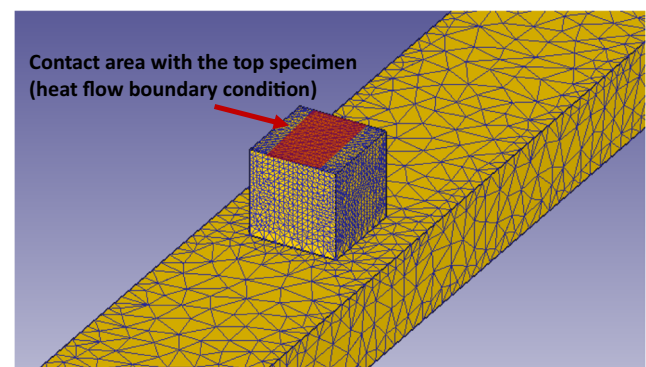


Fig. 4 Bottom specimen mesh used for the thermal analysis

The following constant values were used for the thermal properties of the considered AA2011-T8 and AA6082-T6 aluminum alloys: thermal conductivity 180.2 N/sK, heat capacity 2.433 N/mm²K. The data were taken from the Jmatpro material database. The results of the experimental and numerical campaign described in [25] show that this assumption does not affect significantly the accuracy of the temperature distribution.

Results and discussion

First, a process window was obtained by visual inspection of the joint produced with varying process parameters according to Table 2. Four different categories of welds were identified. In particular, low pressure and low frequency resulted in “Insufficient heat” input into the joint, and no weld could be obtained as the third stage of the process (burn off) could not be activated. Increasing heat input, i.e. increasing oscillation frequency, pressure, or both the parameters, a “Sound” joint was obtained. With further increase of the process parameters values, the excess of heat resulted in a too softened material. In these conditions, the specimens were not able to bear the applied pressure and collapsed completely before the assigned process time was reached. This condition was labeled as “Instability”. Finally, considering the configuration with the AA6082 as top specimen, a limit condition (“Bonding limit”) was found. Although these joints appeared correctly welded by visual inspection, they showed poor mechanical resistance during preliminary testing. These aspects will be better analyzed and described in the following. Figure 5 shows the process window obtained for the two configurations with varying oscillation frequency and interface pressure. In the following of this paragraph, the joint configuration will be referred to indicating the material used for the top specimen followed by the material used for the bottom one. The interface pressure p and oscillation frequency f values used to produce the joint were added to the specimen name in order to completely identify the test, e.g. 6082–2011_30–45 or 2011–6082_30–60.

As it can be seen from Fig. 5, a larger process window was obtained with the 2011–6082 configuration. On the other hand, only one sound joint was produced with the 6082–2011 configuration, while specimens 6082–2011_30–45,

Fig. 5 Process window for the two considered configurations obtained with varying oscillation frequency and interface pressure

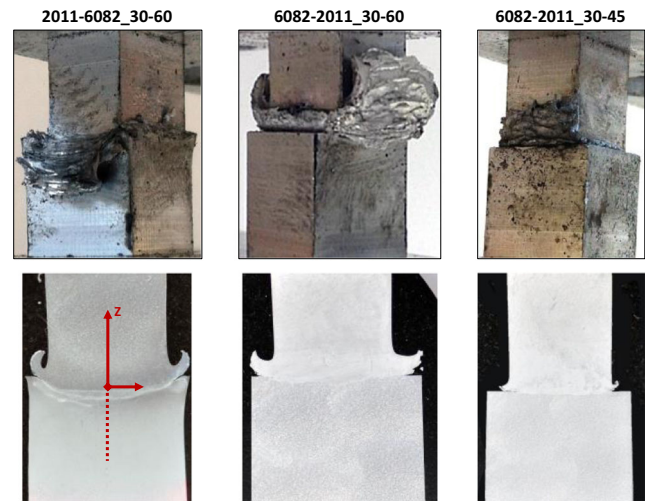
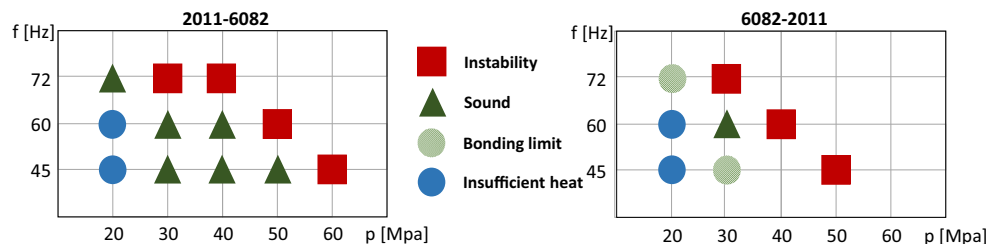


Fig. 6 Pictures of the joints and macro image of the etched cross sections for case studies 2011–6082_30–60, 6082–2011_30–60 and 6082–2011_30–45

6082–2011_40–45 and 6082–2011_20–72 belongs to the “bonding limit” group. Besides, with $f = 45$ Hz and $f = 72$ Hz, an increase in interface pressure, according to the pre-selected values, leads to directly change from “bonding limit” to “instability” with no possibility to obtain sound welds. In order to investigate on the reasons of this behavior, first, microstructure analysis was carried out. In particular, Fig. 6 shows the picture and the macro image of the cross section of joints 2011–6082_30–60, 6082–2011_30–60 and 6082–2011_30–45.

As anticipated, the first two case studies correspond to sound joints while the last, i.e. 6082–2011_30–45, is a “bonding limit” one. In particular, in the macrograph of the etched cross section it can be seen that although material continuity is obtained all along the welding line, almost no flash is generated by the bottom specimen.

Optical microscopy was used to highlight and measure the average grain size of the etched cross sections, in the AA2011 side, according to ASTM E112. Figure 7 shows the typical material zones found moving from the periphery of the joint towards the welding line, i.e. the specimens contact interface, for the 2011–6082_30–60 case study. In particular, base material, Heat Affected Zone (HAZ), Thermo-Mechanically Affected Zone (TMAZ) and Weld Zone (WZ) are encountered as known in literature [13, 14].

Fig. 7 Microstructure of the typical AA2011 material zones in the cross section of the welded specimen: **a** base material, **b** HAZ, **c** TMAZ and **d** WZ

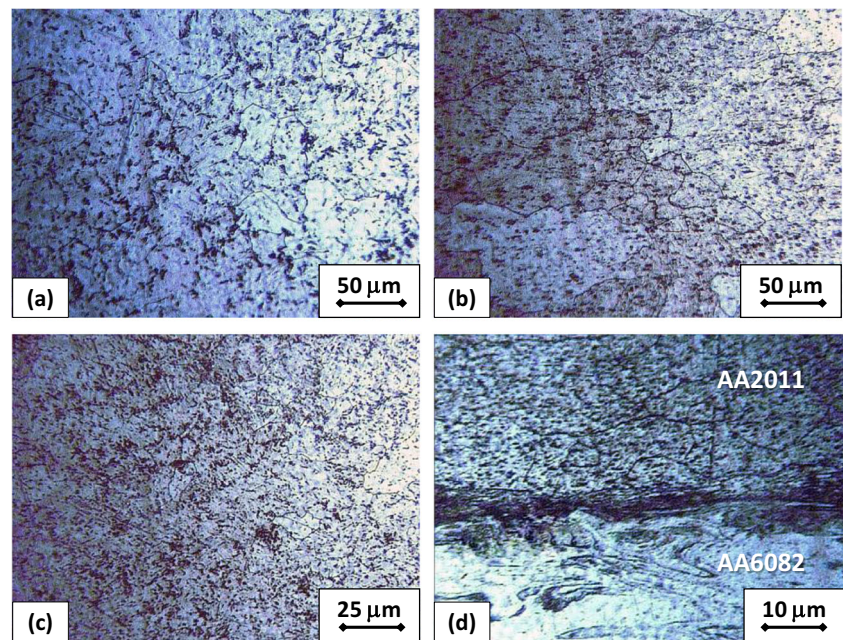
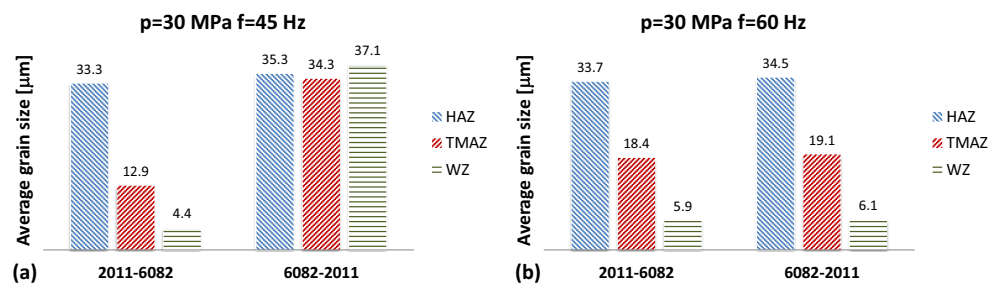


Figure 8 shows the average grain size for the welds obtained with pressure equal to 30Mpa and frequency equal to 45 and 60 Hz, for both the configurations. The average grain size of the base material is 36 μm . It is worth pointing out that the selected etching reagent, i.e. Keller, did not allow to properly highlight the grain size in the 6082 side and grain dimension was measured only in the 2011 side, for both the joint configurations. However, the acquired information permitted to assess whether the used process parameters produced enough heat and deformation to activate the Dynamic Recrystallization Process (DRX), which is usually considered as an indicator of joint integrity in friction based solid state welding processes [2, 13].

Moving towards the WZ a decreasing average grain size is observed. In particular, in the WZ equiaxed grains and size values about one order of magnitude lower than the parent material are found, indicating that the DRX phenomenon took place. This observation does not hold true for the 6082–2011_30–45 case study, i.e. the one labeled as “bonding limit”. For these process conditions, an average grain size similar to the one of the base material is found in all the typical areas of the joint cross section, indicating that no significant microstructural change occurred.

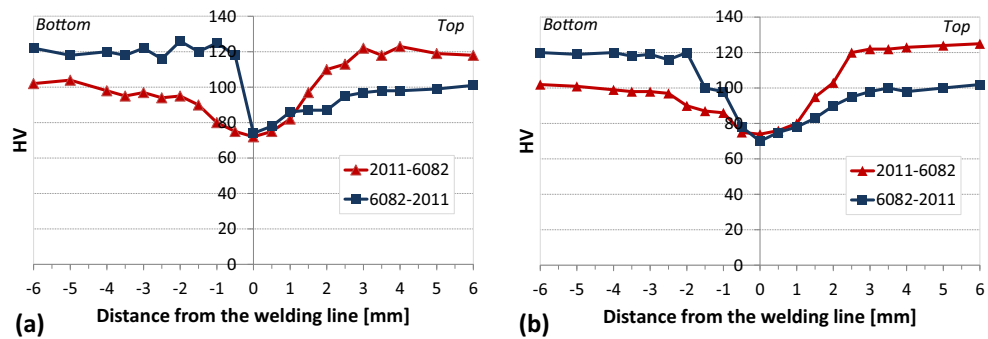
Fig. 8 Average grain size for the welds obtained with **a** $p = 30$ Mpa and $f = 45$ Hz and **b** $p = 30$ Mpa and $f = 60$ Hz



Microhardness was measured along the Z axis (see again Fig. 6). Figure 9 shows the values obtained for the same case studies considered for the grain size analysis.

Again, the 2011–6082_30–45, 2011–6082_30–60, and 6082–2011_30–60 case studies show a similar behavior. In particular, a minimum, equal to about 70 HV, is found on the welding line. Outside this area, microhardness gradually increases until it reaches the values of the two parent materials, i.e. 100 HV for the AA6082-T6 and 120 HV for the AA2011-T8. As the 2011–6082 configuration is regarded, the extension of the area interested by lower hardness with respect to the base material is about 5 mm, almost equally divided in the two materials (2.5 mm on each side). On the other hand, for the 6082–2011_30–60 case study a somewhat smaller extension of this lower hardness zone is found in the bottom specimen, on the AA2011 side. This behavior is dramatically magnified for the 6082–2011_30–45 case study. In these process conditions, a softening similar to the one observed for the other welds is observed in the AA6082 side. In turn, almost no modification is found in the AA2011 side, in which the HV values remain almost constant with decreasing distance from the welding line. It is worth pointing out that lower hardness in the WZ and TMAZ of a joint welded by friction based solid

Fig. 9 Vickers microhardness for the welds obtained with **a** $p = 30$ Mpa and $f = 45$ Hz and **b** $p = 30$ Mpa and $f = 60$ Hz



state techniques, i.e. LFW or FSW, is typical for heat treated alloys. The thermal cycle induced by the process produces temperature values around 80 % of the base material melting temperature. In this way, a loss of hardness is expected and this is not a signal of poor welds. On the contrary, it implies that part of the material close to the welding line participated to the material mixing experiencing large deformation at high temperatures [27, 28].

EDX (Energy-dispersive X-ray spectroscopy) analysis were carried out using a scanning electron microscope in order to highlight the chemical composition along the cross section of the joints. In particular, copper was chosen as element to be investigated as it is found in the chemical composition of AA2011 (about 5 %, see Table 1) and it is almost absent in the chemical composition of AA6082 (about 0.1 %). In this way, the EDX analysis can be used to evaluate the material mixing in the welded joint. Measurements were carried out along the Z axis (see Fig. 6). Figure 10 shows the results obtained for the joints welded with $p = 30$ MPa and $f = 45$ Hz, in both configurations.

A completely different trend is observed for the two considered case studies. As the 2011–6082 configuration is considered, a large amount of copper is found in the bottom specimen, i.e. in the AA6082 side, even at relatively large distance from the welding line. In particular, the copper weight percent increases along the Z axis with the first non zero value found, in the AA6082 side, at a distance of 4 mm from the welding line. On the other hand, almost no copper is found in the top specimen of the 6082–2011 configuration, i.e. the AA6082

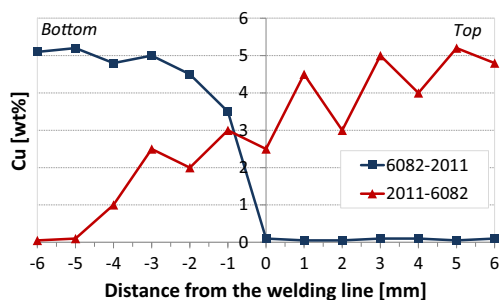


Fig. 10 Cu weight % for the joint welded with $p = 30$ MPa and $f = 45$ Hz

specimen, indicating that proper material mixing did not occur, with detrimental consequences on the joint quality.

For these process conditions, additional tests were performed using the same specimen geometry for the top and bottom specimen. As it could be expected, sound joints were produced regardless of the material positioning. In order to explain the observed behaviors, the numerical model described in the previous paragraph was utilized. It is known that the conditions for effective solid bonding are given by the proper combination of a few variables, namely time, temperature and pressure. According to the Piwnik and Plata criterion, each material has a peculiar threshold value of the integral of the ratio between the normal pressure and the flow stress, being time the variable of integration [29, 30]. The same process time was used for all the tests. Additionally, pressure remained constant for the 2011–6082_30–45 and 6082–2011-30–45 case studies considered in Fig. 10. If the larger dimensions of the bottom element to be welded (see Fig. 2) result in temperatures, close to the specimens contact interface, significantly lower than the ones occurring in the identical specimens geometry conditions, the consequent increased flow stress can determine a lower value of the Piwnik and Plata indicator, thus leading to decreases bonding effectiveness. Figure 11 shows the temperature profiles obtained at the end of the process in the bottom specimen in case of large geometry and small geometry, i.e. same geometry of the top specimen. The heat flow used as boundary condition was

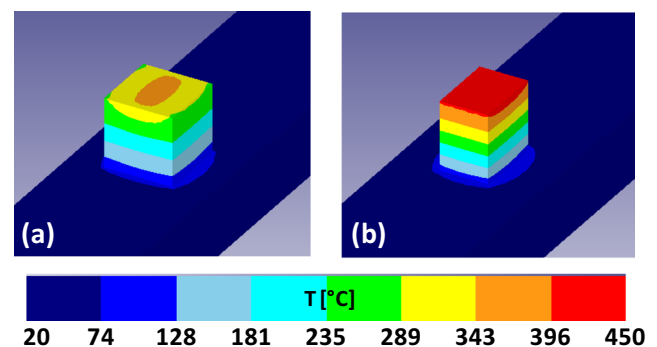


Fig. 11 Temperature profiles in the bottom specimen at the end of the process for **a** large geometry and **b** small geometry

equal to 7000 N/mm s. This value was calculated according to the procedures described in detail in [25] using the same values of pressure and oscillation frequency of the case studies reported in Fig. 10.

A significant difference in the temperature profiles is observed from Fig. 11, due to the larger heat capacity of the large geometry specimen. It should be observed that, provided that the same heat capacity and thermal conductivity are considered for the two alloys [24], the calculated profiles can be considered both for the AA6082 and the AA2011. However, a difference exists between the flow stresses, as a function of temperature, of the two alloys (see Fig. 1). When the bottom specimen is made of AA6082, using the large specimen, a temperature of about 350 °C is found in the welding zone. In these conditions, the flow stress of the AA6082 is about 75 MPa, which corresponds to about 2.5 times the pressure applied. On the contrary, using the AA2011 as bottom specimen material, with the large specimen the flow stress at the contact interface is about 130 MPa, which is about 4.5 times the pressure applied. The consequent decrease in the Piwnik and Plata parameters determines the loss in effectiveness of the joint. Finally, using the small geometry and AA2011 as bottom specimen material, the temperature at the contact interface is about 450 °C, which determines a flow stress of about 75 MPa, recreating conditions very similar to the ones obtained using the large geometry with the AA6082 as bottom specimen material.

Conclusions

In the paper, the results of an experimental and numerical campaign on LFW of dissimilar aluminum alloys are presented. Experimental tests were carried out with fixed process time and oscillation amplitude and varying oscillation frequency, interface pressure and specimens geometry. A thermal numerical model was used to study the temperature profiles in the welded joints. From the obtained results the following main conclusions can be drawn:

- Using the large geometry for the bottom specimen larger process window was obtained when the AA2011 was used as top specimen material. On the contrary, a condition called “Bonding limit” was identified for a few tests carried out with AA6082 as top specimen material;
- Although the “Bonding limit” joints appear effectively welded both by visual inspection of the weld and by optical microscopy of the etched transverse section (material continuity), extremely poor mechanical properties were obtained for these joints;
- Grain size measurements, HV tests and EDX analysis highlighted that in the bonding limit joints no DRX

phenomenon took place, a sharp transition between the hardness of the two materials is found close to the welding line and no material mixing occurs. On the contrary, in the WZ of the sound joints recrystallized grains are found, a smooth transition between the HV values of the two material is observed in an area with extension of about 5 mm and the presence of copper is highlighted in the AA6082 specimen till a distance of about 4 mm from the welding line;

- The calculated temperature fields indicate that low ratios between the applied pressure and the material flow stress are obtained in AA2011 the bottom specimen with large geometry. This configuration produced a “bonding limit” joint. On the other hand, about the same value of the above described ratio is obtained for the AA6082 large geometry bottom specimen and the AA2011 small geometry bottom specimen. Both the later configurations resulted in a sound joint.

The above conclusions permit to derive a few design rules for the LFW of dissimilar joints with different geometries between the top and bottom specimen. In particular, in order to have a larger process window and a more stable process, a key factor is represented by the variation of the flow stress with temperature. When one of the materials has larger flow stress at every temperature, it is preferable to use the harder material for the smaller specimen and the softer material for the larger one.

References

1. Taban E, Gould JE, Lippold JC (2010) Dissimilar friction welding of 6061-T6 aluminum and AISI 1018 steel: properties and microstructural characterization. *Mater Des* 31(5):2305–2311. doi:10.1016/j.matdes.2009.12.010
2. Mishra RS, Ma ZY (2005) Friction stir welding and processing. *Mater Sci Eng R Rep* 50(1–2):1–78P. doi:10.1016/j.mserr.2005.07.001
3. Bhamji I, Preuss M, Threadgill PL, Addison AC (2011) Solid state joining of metals by linear friction welding: a literature review. *Mater Sci Technol* 27(1):2–12
4. Turner R, Gebelin JC, Ward RM, Reed RC (2011) Linear friction welding of Ti-6Al-4 v: modelling and validation. *Acta Mater* 59(10):3792–3803. doi:10.1016/j.actamat.2011.02.028
5. Herbeifuehrung einer Haftverbindung zwischen Plaettchen aus Werkzeugstahl und deren Traegern nach Art einer Schweißung oder Loetung Herbeifuehrung a bond between Flakes made of tool steel and their carriers on the type of welding or soldering (1929). Google Patents,
6. Romero J, Attallah MM, Preuss M, Karadge M, Bray SE (2009) Effect of the forging pressure on the microstructure and residual stress development in Ti-6Al-4 v linear friction welds. *Acta Mater* 57(18):5582–5592. doi:10.1016/j.actamat.2009.07.055
7. Vairis A, Frost M (1998) High frequency linear friction welding of a titanium alloy. *Wear* 217(1):117–131
8. Vairis A, Frost M (1999) On the extrusion stage of linear friction welding of Ti 6al 4 v. *Mater Sci Eng A* 271(1–2):477–484

9. Chamanfar A, Jahazi M, Cormier J (2015) A review on inertia and linear friction welding of Ni-based superalloys. *Metall Mater Trans a* 46(4):1639–1669. doi:[10.1007/s11661-015-2752-4](https://doi.org/10.1007/s11661-015-2752-4)
10. Fratini L, Buffa G, Campanella D, La Spisa D (2012) Investigations on the linear friction welding process through numerical simulations and experiments. *Mater Des* 40:285–291. doi:[10.1016/j.matdes.2012.03.058](https://doi.org/10.1016/j.matdes.2012.03.058)
11. Song X, Xie M, Hofmann F, Jun TS, Connolley T, Reinhard C, Atwood RC, Connor L, Drakopoulos M, Harding S, Korsunsky AM (2013) Residual stresses in linear friction welding of aluminium alloys. *Mater Des* 50:360–369. doi:[10.1016/j.matdes.2013.03.051](https://doi.org/10.1016/j.matdes.2013.03.051)
12. Jun TS, Rotundo F, Song X, Ceschini L, Korsunsky AM (2010) Residual strains in AA2024/AlSiCp composite linear friction welds. *Mater Des* 31(SUPPL. 1):S117–S120. doi:[10.1016/j.matdes.2009.10.004](https://doi.org/10.1016/j.matdes.2009.10.004)
13. Fratini L, Buffa G, Cammalleri M, Campanella D (2013) On the linear friction welding process of aluminum alloys: experimental insights through process monitoring. *CIRP Ann Manuf Technol* 62(1):295–298
14. Ma TJ, Zhong B, Li WY, Zhang Y, Yang SQ, Yang CL (2012) On microstructure and mechanical properties of linear friction welded dissimilar Ti-6Al-4V and Ti-6.5Al-3.5Mo-1.5Zr-0.3Si joint. *Sci Technol Weld Join* 17(1):9–12. doi:[10.1179/1362171811Y.0000000067](https://doi.org/10.1179/1362171811Y.0000000067)
15. Guo Y, Chiu Y, Attallah MM, Li H, Bray S, Bowen P (2012) Characterization of dissimilar linear friction welds of α - β titanium alloys. *J Mater Eng Perform* 21(5):770–776. doi:[10.1007/s11665-012-0129-z](https://doi.org/10.1007/s11665-012-0129-z)
16. Li HY, Huang ZW, Bray S, Baxter G, Bowen P (2007) High temperature fatigue of friction welded joints in dissimilar nickel based superalloys. *Mater Sci Technol* 23(12):1408–1418. doi:[10.1179/174328407X243933](https://doi.org/10.1179/174328407X243933)
17. Dalgaard E, Wanjara P, Trigo G, Jahazi M, Comeau G, Jonas JJ (2011) Linear friction welding of Al-Cu part 2 - interfacial characteristics. *Can Metall Q* 50(4):360–370
18. Wanjara P, Dalgaard E, Trigo G, Mandache C, Comeau G, Jonas JJ (2011) Linear friction welding of Al-Cu: part 1 - process evaluation. *Can Metall Q* 50(4):350–359. doi:[10.1179/000844311X13112418194644](https://doi.org/10.1179/000844311X13112418194644)
19. Bhamji I, Moat RJ, Preuss M, Threadgill PL, Addison AC, Peel MJ (2012) Linear friction welding of aluminium to copper. *Sci Technol Weld Join* 17(4):314–320. doi:[10.1179/1362171812Y.0000000010](https://doi.org/10.1179/1362171812Y.0000000010)
20. Bhamji I, Preuss M, Moat RJ, Threadgill PL, Addison AC (2012) Linear friction welding of aluminium to magnesium. *Sci Technol Weld Join* 17(5):368–374. doi:[10.1179/1362171812Y.0000000017](https://doi.org/10.1179/1362171812Y.0000000017)
21. Rotundo F, Marconi A, Morri A, Ceschini A (2013) Dissimilar linear friction welding between a SiC particle reinforced aluminum composite and a monolithic aluminum alloy: microstructural, tensile and fatigue properties. *Mater Sci Eng A* 559:852–860. doi:[10.1016/j.msea.2012.09.033](https://doi.org/10.1016/j.msea.2012.09.033)
22. Williams JC, Starke Jr EA (2003) Progress in structural materials for aerospace systems. *Acta Mater* 51(19):5775–5799. doi:[10.1016/j.actamat.2003.08.023](https://doi.org/10.1016/j.actamat.2003.08.023)
23. Hirsch J, Al-Samman T (2013) Superior light metals by texture engineering: Optimized aluminum and magnesium alloys for automotive applications. *Acta Mater* 61(3):818–843. doi:<http://dx.doi.org/10.1016/j.actamat.2012.10.044>
24. ASM Specialty Handbook: Aluminum and Aluminum Alloys (1993). ASM International,
25. Buffa G, Cammalleri M, Campanella D, Fratini L (2015) Shear coefficient determination in linear friction welding of aluminum alloys. *Mater Des* in press
26. Bathe KJ (1976) Numerical methods in finite element analysis. Prentice-Hall, Prentice-Hall civil engineering and engineering mechanics series
27. Ola OT, Ojo OA, Wanjara P, Chaturvedi MC (2011) Analysis of microstructural changes induced by linear friction welding in a nickel-base superalloy. *Metall Mater Trans a* 42(12):3761–3777
28. Rotundo F, Ceschini L, Morri A, Jun TS, Korsunsky AM (2010) Mechanical and microstructural characterization of 2124Al/25 vol.%SiCp joints obtained by linear friction welding (LFW). *Compos Part A-Appl S* 41(9):1028–1037. doi:[10.1016/j.compositesa.2010.03.009](https://doi.org/10.1016/j.compositesa.2010.03.009)
29. Buffa G, Pellegrino S, Fratini L (2014) Analytical bonding criteria for joint integrity prediction in friction stir welding of aluminum alloys. *J Mater Process Technol* 214(10):2102–2111. doi:[10.1016/j.jmatprotec.2014.02.014](https://doi.org/10.1016/j.jmatprotec.2014.02.014)
30. Plata M, Piwnik J Theoretical and experimental analysis of seam weld formation in hot extrusion of aluminum alloys. In: 7th Int. Al. Extr. Tech. Sem, 2000. pp 205–211